

Vacancies, interstitials, and close Frenkel pairs on the zinc sublattice of ZnSe

F. C. Rong,^{*} W. A. Barry,[†] J. F. Donegan,[‡] and G. D. Watkins

Department of Physics, Lehigh University, 16 Memorial Drive East, Bethlehem, Pennsylvania 18015

(Received 18 March 1996; revised manuscript received 15 May 1996)

Zinc vacancies (V_{Zn}), zinc interstitials (Zn_i), and ~ 25 distinct V_{Zn} - Zn_i Frenkel pairs of different lattice separations are observed in ZnSe by the optical detection of magnetic resonance in photoluminescence after 2.5 MeV electron irradiation *in situ* at 4.2 K. The stability, photoluminescence energy, anisotropy of production vs beam direction, plus exchange and dipole-dipole interactions in the excited emitting state are measured directly for most of the pairs. Combining this with information previously determined for the isolated vacancy and interstitial, the electronic and lattice structures of the defects and their role in the various luminescence processes are established. The second-donor level (+/2+) for Zn_i is estimated to be at $E_C - 0.9$ eV. [S0163-1829(96)04736-4]

I. INTRODUCTION

In the present paper, we describe optical detection of magnetic resonance (ODMR) studies in the photoluminescence of ZnSe after irradiation by 2.5 MeV electrons *in situ* at 4.2 K. Observed, frozen into the lattice after the primary displacement event, are zinc vacancies, zinc interstitials, and 25 well resolved distinct close zinc-interstitial-zinc-vacancy Frenkel pairs of varying separation in the lattice. This study has been in progress over a number of years and some of the highlights have been described in short communications over this extended period.¹⁻⁵ The purpose of the present paper is to supplement these results with recent and previously unpublished results, and to fold them into our present understanding of this interesting system.

The outline of the paper is as follows: In Sec. II, we describe the experimental details for the *in situ* electron irradiation and ODMR experiments. In Sec. III, we briefly review what has been established concerning the isolated vacancy from previous EPR and ODMR studies, and the early evidence for Frenkel pairs from EPR studies. We supplement this with some relevant previously unpublished results. In Sec. IV, we summarize briefly the ODMR results for interstitial zinc in the T_d site surrounded by four Se neighbors, and present results for the less stable site (tentatively identified) surrounded by four Zn's. The wave function of the unpaired electron on Zn_i^+ in the more stable site is analyzed and used to provide an approximate estimate of the electrical level position of its Zn_i^+/Zn_i^{2+} double-donor level in the band gap. In Sec. V, we describe ODMR results for eight distant Frenkel pairs, bringing the total now to 25. In all cases, the ODMR spectra can be analyzed as reflecting the sum of the $S = 1/2$ spin Hamiltonians of the isolated vacancy and interstitial plus an exchange and a weaker dipole-dipole interaction between them, and we supply a more complete analysis of these terms for several of the previously reported closer pairs. In this section, we also describe in detail the results of defect alignment vs bombarding electron beam direction, which has allowed tentative assignments of a few of the defects to specific lattice sites. One of these has allowed, in turn, another independent estimate for the interstitial double-donor level which is generally consistent with that

estimated in Sec. IV, but is believed to be more accurate. Section VI presents a summary of the results and our present understanding of these intrinsic defects on the zinc sublattice.

In an accompanying paper that immediately follows this,⁶ advantage will be taken of this unique system to measure the radiative lifetimes of several of the individual Frenkel pairs. This information, related to the overlap of vacancy and interstitial wave functions in a manner similar to that for the exchange interaction, also provides important clues concerning the separations of the pairs. Theoretical treatments of the exchange and radiative lifetimes will also be presented there, leading finally to tentative lattice assignments for all of the pairs.

II. EXPERIMENTAL PROCEDURE

The ODMR experiments were performed at 20 GHz in an EPR spectrometer cryostat assembly fitted with 0.001 in. titanium windows for *in situ* irradiation by electrons from the Lehigh University 2.5 MeV Van de Graaff accelerator. During the irradiation, the sample was immersed in liquid helium (4.2 K), and afterward was lowered into the center of a TE₀₁₁ microwave cavity for study with the liquid pumped below the λ point (~ 1.5 K). Optical excitation of ~ 5 mW was provided by the 458 or 476 nm line of an argon ion laser through an optical fiber terminating at a point on axis in the cavity just above the sample. The fiber was threaded through a concentric quartz capillary tube (3/16 in. diam \times 48 in. long) which served as a light pipe to guide the luminescence out of the cryostat to an external silicon diode (EG&G 250 UV) or a cooled germanium detector (North Coast EO-817S).

Microwaves from a 300 mW Gunn diode oscillator (CMC model CME624AD) were on-off modulated by a PIN-diode and fed to the microwave cavity, the resulting changes in luminescence being detected synchronously by a lock-in amplifier. The lock-in output was recorded either by an XY recorder or digitized and sent to a PC for signal averaging and other digital processing. The spectral dependence of an ODMR signal was performed by inserting a 1/4 meter Jarrell-Ash monochromator between the lightpipe and detec-

tor and scanning the wavelength while tuned to the signal of interest.

The samples studied were single crystals grown by vapor transport in a sealed quartz ampoule, and most were supplied by Manuel Aven at General Electric Research and Development Center. Some were supplied by Brian Fitzpatrick at Philips Laboratory. Both as-grown (high resistivity) and zinc-fired (low resistivity) n -type samples were studied. For the studies of defect alignment vs bombarding electron beam direction, the $[111]$ and $[\bar{1}\bar{1}\bar{1}]$ directions were determined from the surface etching behavior in hot NaOH of suitably thinned samples, as described in previous EPR alignment studies.⁷

III. REVIEW OF THE ZINC VACANCY

A. The isolated vacancy

The following properties for the isolated zinc vacancy have been established.⁷⁻¹⁵ It introduces a double acceptor level ($2-/-$) in the ZnSe energy gap. In its V_{Zn}^- charge state it is paramagnetic and its EPR reveals the trapped hole highly localized on a single Se neighbor, primarily p like and pointing into the vacancy. This results from a trigonal Jahn-Teller distortion in which the atom containing the hole relaxes into the vacancy. Combining optical, ODMR and EPR studies, it has been possible to construct a complete configurational coordinate diagram for both charge states of its double-acceptor level, from which the magnitude of the V_{Zn}^- Jahn-Teller energy is determined to be 0.35 eV, and the double acceptor level position to be at $E_V + 0.66$ eV.¹⁵

The EPR of V_{Zn}^- is described by the $S=1/2$ spin Hamiltonian,

$$\mathcal{H}_V = \mu_B \mathbf{S}_V \cdot \mathbf{g}_V \cdot \mathbf{B} + \mathbf{S}_V \cdot \sum_j (\mathbf{A}_V)_j \cdot \mathbf{I}_j, \quad (1)$$

where $(\mathbf{A}_V)_j$ is the hyperfine interaction tensor with ⁷⁷Se ($I=1/2$, 7.8% abundant) at the j th neighbor site. (The subscript V has been added to distinguish between a similar Hamiltonian for the zinc interstitial, to be introduced later.) The values for \mathbf{g}_V , and $(\mathbf{A}_V)_j$ are given in Table I, with the principal axes defined in Fig. 1, where a , b , c , and d can be considered the four Se atoms surrounding the vacancy. As defined, \mathbf{A} in the table gives the major hyperfine interaction on atom c in the figure, which contains the hole. Included also are weaker ⁷⁷Se hyperfine interactions, not previously reported, for two sets of three equivalent additional neighbors (total of six), labeled \mathbf{A}' and \mathbf{A}'' , derived from complex partially resolved satellite structure on each of the main EPR transitions. In Fig. 1, the principal axes are indicated for one of the three equivalent sets (rotation around $[111]$ by $\pm 120^\circ$) of each. One set presumably arises from the three remaining neighbors to the vacancy (a , b , and d in Fig. 1), the other most likely from three equivalent selenium neighbors at the same distance behind atom c . An LCAO treatment of \mathbf{A} , \mathbf{A}' , and \mathbf{A}'' , assuming the components to be unchanged in sign for each (not determined), gives, using the Hartree-Fock estimates of Koh and Miller¹⁶ for Zn^- , $\sim 75\%$ of the hole wave function on atom c with $\sim 3\%$ and $\sim 5\%$ on each of the three atoms associated with \mathbf{A}' and \mathbf{A}'' , respectively, adding

TABLE I. Spin Hamiltonian parameters for the isolated zinc vacancy and interstitial. The defect principal axes are indicated in Fig. 1. $[(Zn_i^+)^*]$ is tentatively identified as interstitial zinc in the less stable site surrounded by four zinc atoms, with six Se atoms at the second nearest neighbor positions.]

Spectrum (defect)	\mathbf{g}	$\mathbf{A}({}^{77}\text{Se})$ (MHz)	$\mathbf{A}({}^{67}\text{Zn})$ (MHz)
V	$g_1 = 1.9548(2)$	$A_1 = 802(2)$	
(V_{Zn}^-)	$g_2 = 2.2085(2)$	$A_2 = 150(1)$	
	$g_3 = 2.2085(2)$	$A_3 = 150(1)$	
	$\tau = 0^\circ$	$\tau = 0^\circ$	
		$A'_1 = 65(2)$	
		$A'_2 = 39(2)$	
		$A'_3 = 34(2)$	
		$\eta' = 9(2)^\circ$	
		$A''_1 = 65(2)$	
		$A''_2 = 21(2)$	
		$A''_3 = 16(2)$	
		$\eta'' = 39(2)^\circ$	
Zn_i^+	$g_0 = 1.9664(4)$	$A(1\text{ nn})_{\parallel} = 514(3)$	$A_0 = 1088(15)$
		$A(1\text{ nn})_{\perp} = 464(3)$	
		$(\parallel = 4 \langle 111 \rangle \text{'s})$	
		$A(3\text{ nn})_0 = 37(3)$	
$(Zn_i^+)^*$	$g_0 = 2.0064(5)$	$A(2\text{ nn})_{\parallel} = 235(20)$	
		$A(2\text{ nn})_{\perp} = 185(20)$	
		$(\parallel = 6 \langle 100 \rangle \text{'s})$	

up to a total of $\sim 100\%$. Since \mathbf{A}' and \mathbf{A}'' are of comparable magnitude, we do not attempt here to assign them, although in a previous reference to these unpublished results, the orientation of their principal axes was used as a reasonable argument to assign \mathbf{A}' to a , b , and d .¹⁵

The spin lattice relaxation time T_1 for the vacancy has also been determined, using the transient recovery under an adiabatic fast passage technique.¹⁷ The results, also not previously published, are 0.023 sec at 4.2 K and 0.35 sec at 1.5 K.

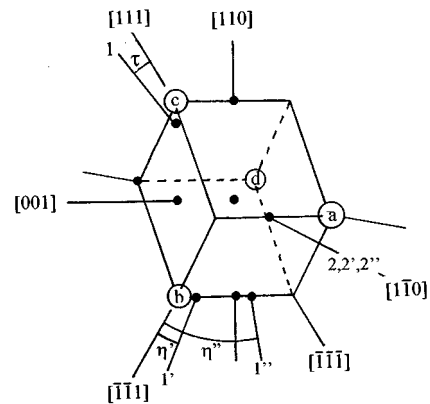


FIG. 1. Principal axes of the spin Hamiltonian parameters for V_{Zn}^- and the Frenkel pairs. The defect orientation shown is labeled bc , see text.

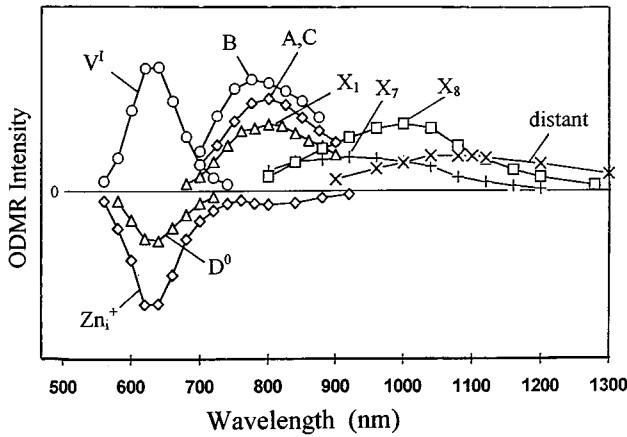


FIG. 2. Spectral dependences of several of the prominent ODMR signals.

B. Vacancies perturbed by nearby interstitials

In the early EPR studies, electron irradiation *in situ* at 20.4 K was also observed to produce zinc-vacancy–zinc-interstitial close Frenkel pairs, as evidenced by the presence of V_{Zn}^- -like EPR spectra as perturbed by a nearby interstitial Zn_i^{2+} atom.^{7,18} Four distinct pairs were resolved, and combining information obtained from their alignment vs electron bombardment direction, detailed microscopic models were deduced for three of them. The dominant one, V^I , was identified as arising from an interstitial in the easy $[111]$ displacement direction at 4.89 Å separation, and V^{III} as arising from an interstitial in a $\langle 100 \rangle$ direction at either the closest such site at 2.83 Å, or at the next, at 8.48 Å. (These are the nearest interstitial sites in the appropriate directions which are surrounded by four seleniums, assumed to be the more stable sites). V^{II} emerged when V^I anneals at ~ 80 K, and combining this with correlated alignment between the two led to its identification as that of the interstitial in a stable site also at 4.89 Å, but in the $[111]$ direction from the vacancy, with a selenium nearest neighbor of the vacancy between.

IV. ISOLATED INTERSTITIAL ZINC

A. Experimental results

Interstitial Zn_i^+ has been observed by ODMR as a negative signal in a strong 625 nm luminescence band produced by 2.5 MeV electron irradiation at 4.2 K.^{1,5} The band was identified as arising from distant shallow donor to the V^I closest Frenkel pair acceptor (positive signals) recombination luminescence, and the negative interstitial signal was interpreted as resulting from competitive donor to interstitial recombination. The spectral dependences of the donor and V^I resonances are presented in Fig. 2, along with those of other spectra to be described in the following sections, confirming this assignment.

Assignment of the spectrum to isolated interstitial Zn_i^+ in the stable site surrounded by four seleniums, resulted from its isotropic g value, plus direct ODMR detection of hyperfine interactions with the central ^{67}Zn ($I=5/2$, 4.1 % abun-

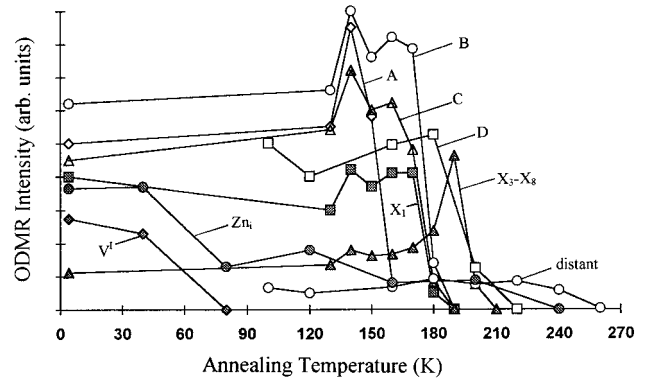


FIG. 3. Amplitudes of the individual ODMR spectra vs isochronal (15 min) annealing.

dant) and ^{77}Se ($I=1/2$, 7.8 % abundant) at the four nearest and twelve third nearest neighbor sites. The appropriate spin Hamiltonian is given by

$$\mathcal{H}_I = g_I \mu_B \mathbf{S}_I \cdot \mathbf{B} + \mathbf{S}_I \cdot \sum_j (\mathbf{A}_I)_j \cdot \mathbf{I}_j, \quad (2)$$

and the parameters are also listed in Table I. Also observed was an isotropic weaker negative signal with partially resolved shoulders consistent with hyperfine interactions for six equivalent ^{77}Se neighbors. This spectrum was not stable and disappeared over a period of several hours at 4.2 K during the optical excitation associated with the ODMR studies. The spin Hamiltonian parameters of this spectrum, tentatively identified with Zn_i^+ in the other, less stable, site surrounded by four zincs and six next nearest seleniums,¹ are presented for the first time also in Table I, and listed as $(Zn_i^+)^*$.

Although the 625 nm luminescence disappears at ~ 80 K (consistent with the observation for V^I), the Zn_i^+ spectrum can still be observed as a negative signal on a remaining weaker 600 nm luminescence, originally present, which is associated with donor to A-center “self-activated” recombination. The Zn_i^+ resonance is stable vs annealing up to ~ 240 K, where it disappears. The annealing results are shown in Fig. 3, along with those for several other spectra to be described in the following sections.

A search of the luminescence over the spectral regions 500–1350 nm and 1400–1900 nm revealed no region where the Zn_i^+ ODMR signal is positive. The region 1350–1400 nm is excluded due to the characteristic water absorption bands in our long quartz pipe. We can conclude therefore either that (1) the donor to Zn_i^+ recombination is nonradiative, (2) it is radiative with $h\nu < 0.65$ eV, or (3) it is radiative in the 1350–1400 nm blind region. We mention this third possibility because in a separate luminescence study with thin optical windows, we have detected a luminescence band with a strong zero phonon line at 0.907 eV (Huang-Rhys factor $S \sim 1$) after electron irradiation at 30 K. This spectrum is shown in Fig. 4. It disappears upon annealing in the same general temperature region (~ 220 K) as the Zn_i^+ ODMR signal, which is suggestive.

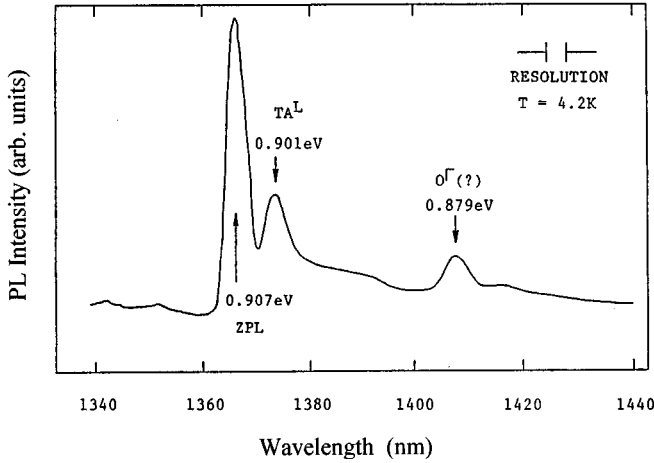


FIG. 4. Photoluminescence band produced in ZnSe by electron irradiation at 30 K to a fluence of $1.3 \times 10^{17} e/cm^2$. It disappears after annealing at ~ 220 K.

B. Analysis of the wave function

The simplest analysis for representing the electronic wave function for such a center is using the linear combination of atomic orbital (LCAO) approximation.¹⁹ Such an analysis was performed in an earlier paper¹ giving, from the hyperfine interactions on the various shells, 60% on the central Zn, 20% on the four nearest Se neighbors, and 3% on the second Se shell. Repeating this with the free atom and ion Hartree-Fock estimates of Koh and Miller,¹⁶ the results become 65%, 32%, and 3%, respectively. In either case, the conclusions are the same — that the wave function is highly localized, indicating a deep center in the gap.

Here, we present an alternative approach which has the advantage that it provides an approximate measure of the level position in the gap. This method, often used for isotropic color centers in ionic crystals,^{20,21} starts with a spherically symmetric one-electron envelope function $\Phi(r)$ for the electron, which is subsequently orthogonalized to the ion cores of the lattice atoms to give

$$\psi(\mathbf{r}) = N \left[\Phi(r) - \sum_{j,\alpha} \phi_j^\alpha \langle \phi_j^\alpha | \Phi(r) \rangle \right]. \quad (3)$$

Here, α denotes each of the core orbitals on atom j , N is a normalization factor, and overlap integrals between ion core orbitals have been ignored. Here, as in the LCAO approximation, the major contribution to the hyperfine interaction at the j site comes from the ϕ_j^α core orbitals, which we estimate as follows: We assume a slowly varying envelope function over the extent of each of the core orbitals, giving

$$\langle \phi_j^\alpha | \Phi(r) \rangle \cong \Phi(r_j) \int \phi_j^\alpha dV. \quad (4)$$

Combining Eqs. (3) and (4) gives

$$|\psi(r_j)|^2 \cong G_j N^2 |\Phi(r_j)|^2, \quad (5)$$

where

$$G_j = \left| 1 - \sum_{\alpha} \phi_j^\alpha(0) \int \phi_j^\alpha dV \right|^2. \quad (6)$$

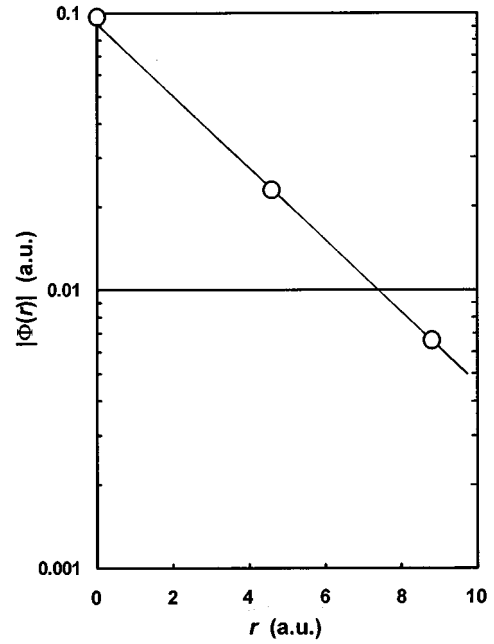


FIG. 5. Amplitude of the $\Phi(r)$ envelope wave function for Zn_i^+ vs r deduced from hyperfine interactions with the central zinc and its first two shells of selenium neighbors.

We use the experimental isotropic hyperfine constants a_j to estimate $|\psi(r_j)|^2$ using¹⁹

$$a_j = \frac{1}{3} \{ (A_{\parallel})_j + 2(A_{\perp})_j \} = (16\pi/3) (\mu_j/I_j) \mu_B |\psi(r_j)|^2, \quad (7)$$

where μ_j and I_j are the nuclear magnetic moment and spin of the j th nucleus, and μ_B the Bohr magneton. We then calculate G_j using self-consistent Hartree-Fock functions for the free Zn^{2+} and Se^0 ions,²² and, with Eq. (5), determine $|\Phi(r_j)|$. The result is shown in Fig. 5. [The straight line drawn through the three points corresponds to a simple exponential drop off vs r , which, in turn, allows a straight forward determination of N to be 0.93, which has been used in the evaluation of $|\Phi(r_j)|$.]

Theoretically, we might expect the one-electron envelope function for the unpaired electron of Zn_i^+ to be close to that of a $Z=2$ hydrogen atom (He^+) in a uniform dielectric. The appropriate dielectric constant for ZnSe should be somewhere between²³ $\epsilon_0 = 8.8$ and $\epsilon_{\infty} \sim 6$, presumably closer to ϵ_{∞} for such a deep electronic state, and, similarly for a deep defect, the electron mass should be close to the free electron mass m . This problem has the simple solution

$$\Phi_{He^+}(r) = \frac{1}{(\pi a_0^3)^{1/2}} \exp(-r/a_0), \quad (8)$$

with the binding energy given by

$$E = 2me^4/\epsilon^2\hbar^2 = e^2/\epsilon a_0 \quad (9)$$

and a Bohr radius

$$a_0 = \frac{\epsilon\hbar^2}{2me^2} = \frac{\hbar}{\sqrt{2m|E|}}. \quad (10)$$

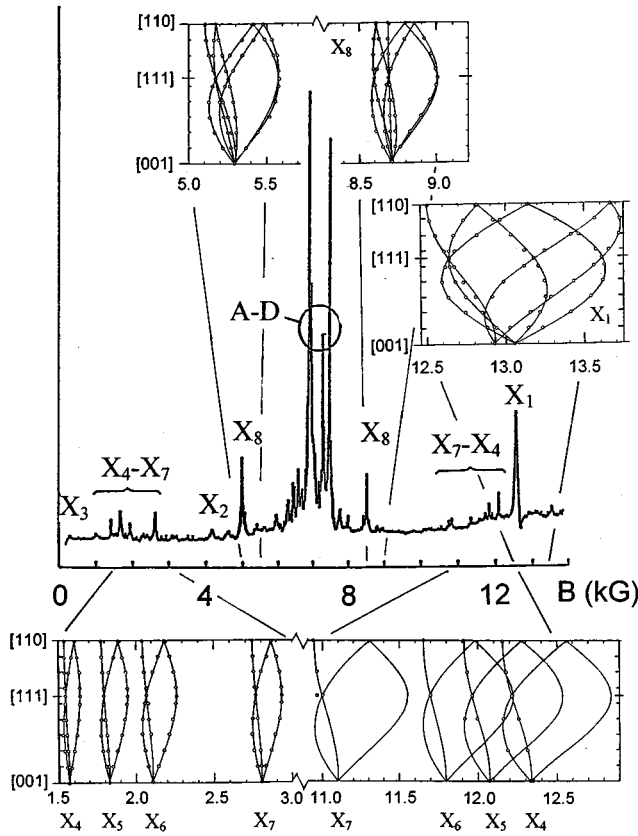
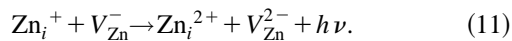


FIG. 6. ODMR spectrum observed in the photoluminescence with $\lambda > 700$ nm. The insets show the angular dependences in the $(1\bar{1}0)$ plane for several of the prominent Frenkel pairs.

The slope of the straight line connecting the points of Fig. 5 gives $a_0 = 1.78 \text{ \AA}$, corresponding to $\epsilon = 6.74$, a reasonable value, and a binding energy of 1.2 eV. This simple very approximate treatment suggests therefore the second-donor level $(+2+)$ for interstitial zinc to be at $\approx E_C - 1.2$ eV.

V. ODMR OF FRENKEL PAIRS

The ODMR spectrum observed in the broad spectral region $\lambda > 700$ nm is shown in Fig. 6. All of the many spectral lines, which spread over the full available magnetic field range, can be shown to arise from the zinc-interstitial donor to its partner vacancy acceptor recombination for Frenkel pairs of different separations, i.e.,



A. Analysis of the spectra

For the excited emitting state observed by ODMR, the spin Hamiltonian can be approximated accurately by^{3,5}

$$\mathcal{H} = \mathcal{H}_V + \mathcal{H}_I + 2\mathbf{S}_V \cdot \mathbf{D} \cdot \mathbf{S}_I + J\mathbf{S}_V \cdot \mathbf{S}_I, \quad (12)$$

where the first two terms are the spin Hamiltonians for isolated V_{Zn}^- and isolated Zn_i^+ , respectively, the third term, a ‘‘dipole-dipole’’-like interaction between the spins of the hole (\mathbf{S}_V) on the vacancy and the electron (\mathbf{S}_I) on the inter-

TABLE II. Spin Hamiltonian parameters (A and D values in MHz) for the $S=1$ Frenkel pairs. The principal axes are denoted in Fig. 1.

	$A(V^{IV})$ (C_{3v})	$B(V^{III})$ (C_{1h})	C ($< C_{3v}$)	D (C_{3v})
g_1	1.960(1)	1.943(1)	1.960(1)	1.960(1)
g_2	2.083(2)	2.082(2)		2.087(2)
g_3	2.083(2)	2.082(2)		2.087(2)
τ_g	0°	0°	0°	0°
D_1	$\pm 294(6)$	$\pm 546(6)$	$\pm 366(10)$	$\pm 90(10)$
D_2	$\mp 147(3)$	$\mp 528(6)$		$\mp 45(5)$
D_3	$\mp 147(3)$	$\mp 18(6)$		$\mp 45(5)$
τ_D	0°	$-10(2)^\circ$		0°
$^{77}\text{A}_{\parallel}$	405(30)	405(30)	405(30)	
$^{77}\text{A}_{\text{iso}}$	225(15)	225(15)	225(15)	
Anneal T (K)	160	180	180	200
λ_{max} (nm)	800	775	800	860

stitial, and the last term, an isotropic exchange interaction between the two spins. This can be rewritten as

$$\begin{aligned} \mathcal{H} = & \mu_B \mathbf{S} \cdot \left[\frac{\mathbf{g}_V + \mathbf{g}_I}{2} \right] \cdot \mathbf{B} + \mathbf{S} \cdot \left[\sum_j \frac{(\mathbf{A}_V)_j + (\mathbf{A}_I)_j}{2} \cdot \mathbf{I}_j \right] + \mathbf{S} \cdot \mathbf{D} \cdot \mathbf{S} \\ & + [S(S+1) - 3/2]J/2 + \mu_B (\mathbf{S}_V - \mathbf{S}_I) \cdot \left[\frac{\mathbf{g}_V - \mathbf{g}_I}{2} \right] \cdot \mathbf{B} \\ & + (\mathbf{S}_V - \mathbf{S}_I) \cdot \left[\sum_j \frac{(\mathbf{A}_V)_j - (\mathbf{A}_I)_j}{2} \cdot \mathbf{I}_j \right], \end{aligned} \quad (13)$$

where $\mathbf{S} = \mathbf{S}_V + \mathbf{S}_I$, and $S = 1$, or 0.

The first three terms commute with \mathbf{S} , and have only diagonal matrix elements within the $S=1$ or 0 manifolds, which are separated in energy by J , as given by the fourth term. The last two terms are off-diagonal and serve to mix the $S=1$ and 0 states. Therefore, if $|J| \gg \mu_B |\mathbf{g}_V - \mathbf{g}_I| B$ or $|A_{V,j}|$, as can be expected for the very close pairs, S is a good quantum number and the first three terms form the relevant Hamiltonian, only slightly perturbed by the off-diagonal terms. This is the case for the strong lines in the center, which have been shown to arise from four distinct $S=1$ centers, labeled $A-D$. The spin Hamiltonian parameters for these spectra, previously reported^{2,3} but updated now to include the analysis of \mathbf{D} for each, are given in Table II. [Consistent with Eq. (13), and Table I, their \mathbf{g} tensors are seen to be very close to the average of those for isolated V_{Zn}^- and Zn_i^+ , as are the hyperfine tensors, which could be resolved for the more intense $A-C$ spectra, with $^{77}\text{A}_{\parallel}$ and $^{77}\text{A}_{\text{iso}}$ one-half of the values for V_{Zn}^- and Zn_i^+ , respectively. The \mathbf{g} and \mathbf{A} tensors do not therefore reveal the orientation of the pair in the lattice, always reflecting instead the $\langle 111 \rangle C_{3v}$ symmetry of V_{Zn}^- . It is only the \mathbf{D} term that potentially contains this information. We note also that the presence of the Zn_i^+ four nearest ^{77}Se hyperfine interactions confirms

that for these pairs the interstitial is also in the stable site surrounded by four selenium neighbors.

If $|J|, |D| \ll \mu_B |\mathbf{g}_V - \mathbf{g}_I| B$ or $|A_{V,I}|$, as expected for the distant pairs, Eq. (12) is the proper starting point and the situation is again simple. In this case, the correct eigenstates of the system are the products of the separate solutions of \mathcal{H}_V and \mathcal{H}_I and the first order effect of the \mathbf{D} and J terms is to introduce a correction to the energies of $(J + D_1 n_1^2 + D_2 n_2^2 + D_3 n_3^2) m_V m_I$, where n_1, n_2, n_3 are the direction cosines of \mathbf{B} , with respect to the 1,2,3 principal axes of \mathbf{D} . The ODMR spectrum is therefore made up of the separate $\Delta m_{V,I} = \pm 1$ transitions for the isolated vacancy and isolated interstitial but with each of the lines split by $|J + D_1 n_1^2 + D_2 n_2^2 + D_3 n_3^2|$, allowing a direct measurement of J and \mathbf{D} . If, however, J is comparable to the other terms, the complete Hamiltonian of Eq. (13) is required.

The general behavior is therefore as follows. At vanishing $|J|$, the spectra of the isolated vacancy and interstitial are observed. Initially, as $|J|$ increases, each of the lines split by $|J + D_1 n_1^2 + D_2 n_2^2 + D_3 n_3^2|$. (The \mathbf{D} term is only important for the closer pairs.) As $|J|$ increases further, the lines in the middle converge and become the $\Delta M_S = \pm 1$ transitions within the $S = 1$ manifold, and the other lines, which become the "forbidden" $\Delta S = \pm 1$ transitions continue to split out, sweeping across and ultimately out of the available magnetic field range. (An illustrative plot of this dependence on $|J|$ is given in Refs. 3,5.) If observed in a normal EPR experiment, these $\Delta S = \pm 1$ transitions would become very weak, due to their strongly reduced transition probability. However, in ODMR, they can remain strong because we are well into microwave saturation conditions, and the transitions serve to take the system out of the bottleneck $S = 1$ states to the radiative $S = 0$ states, giving strong signals.

With the exception of the central $A-D$ spectra, all of the remaining lines visible in Fig. 6 arise from these outer "forbidden" $\Delta S = \pm 1$ transitions, which, for $|J| < \mu_B |\mathbf{g}_V + \mathbf{g}_I| B$, occur by pairs around the central region, as shown for X_4-X_8 . For X_1-X_3 , $|J|$ is larger and the high field transition is out of the magnetic field range. The angular dependences for the prominent ones are shown in the figure, and the spin Hamiltonian parameters for these, and all others that have ultimately been resolved, are included in Table III. In the table we present the analysis of \mathbf{D} for X_1-X_8 and include eight additional distant pairs to those previously reported.

In Fig. 7, we show the spectra in the central region where the transitions for these more distant pairs occur. (The $S = 1$, $A-D$ spectra, dominant in Fig. 6, have been suppressed by accepting only luminescence with $\lambda > 950$ nm. Further suppression has also been achieved because of angular dependence for the $A-D$ intensities, common for $S = 1$ ODMR signals, giving weaker signals for $\mathbf{B} \parallel [001]$.) We note that as the on-off microwave modulation frequency is changed, the spectra also change. Lines grow and decay at different rates and ultimately at the lowest frequency, the only remaining lines are at the positions of the isolated vacancy and interstitial positions. We will see in the following paper (II) that this reflects different radiative lifetimes for the different pairs and will serve as a direct measure of these lifetimes. Here we have simply taken advantage of this to separate out the prominent spectra in this region, some of

which are identified in Fig. 7(c). Using this technique, it was possible to extract the eight additional Frenkel pairs in Table III. These are indicated by an asterisk in the table, which now includes 20 distinct pairs, ordered by their measured exchange, plus pairs distant enough so that exchange splittings are negligible and the isolated vacancy and interstitial spectra are observed.

With the exception of X_1 , with the largest measured $|J|$, the g values for all twenty pairs are accurately given by the isolated vacancy and interstitial values, as expected. (In the case of X_1 , only the lower field $\Delta S = \pm 1$ transition is observed, so a complete analysis was not possible. The values given in the table match the experimental angular dependence of the spectrum, and result from requiring the least departure from $\mathbf{g}_e = \mathbf{g}_I$ and $\mathbf{g}_h = \mathbf{g}_V$ in the analysis. The rather large angular dependence observed for X_1 has required a large value for \mathbf{D} , plus a small residual departure for g_{h1} , which is well within the variations observed by EPR for the very close Frenkel pairs.⁷ However, the large \mathbf{D} is unexpected, being substantially larger than those for the $A-D$ pairs assigned to the nearest separations in Table II. Alternative analyses, allowing departures from \mathbf{g}_I and \mathbf{g}_V , can reduce \mathbf{D} , or even remove it completely, but then the required departures in \mathbf{g}_I and \mathbf{g}_V appear larger than expected. In the absence of the other $\Delta S = \pm 1$ transition, these uncertainties unfortunately cannot be resolved.) In addition, X_4 and X_8 are strong enough to resolve the same ⁷⁷Se hyperfine structure as seen on the A, B , and $C, S = 1$ spectra — an anisotropic pair of satellites of intensity corresponding to a single Se site and inner isotropic satellites corresponding to four equivalent sites. In this case, the splittings are different on the high and low field transitions for each, reflecting the different vacancy and interstitial contributions to the states involved in the transitions when $|J| \sim \mu_B |\mathbf{g}_V - \mathbf{g}_I| B$, but taking this into account, they reveal again the full isolated vacancy and interstitial (surrounded by four seleniums) values.

In Table III, we have listed the values of $|J|$, avoiding a sign assignment, although we might anticipate a negative sign for $s = 1/2$ particles with weakly overlapping wave functions. Direct evidence that it is indeed negative is provided also in slightly weaker intensities evident in Fig. 6 for the high vs the low field transitions for each of the X_3-X_8 spectra. We defer this argument to the following paper (II), however, where the dynamics of the ODMR transitions supply a stronger argument.

B. Defect production with an oriented electron beam

In a primary damage event, the incoming electron transmits the maximum recoil energy to an atom when it recoils in the direction of the bombarding electron. As a result, the Frenkel pairs should show a strong correlation between their orientation in the lattice and the bombarding beam direction, as observed in the earlier EPR studies⁷ described in Sec. III. Along the $[111]$ direction of the zinc blende ZnSe lattice, the atoms are aligned in the sequence Zn-Se-X-X-Zn-Se-X-X, where X denotes vacant interstitial sites. Therefore, the easy recoil direction for a zinc atom is the $[\bar{1}\bar{1}\bar{1}]$ direction, and the difficult direction, blocked by a Se atom, is the $[111]$. Because, in the angular dependence studies, the individual

TABLE III. Spin Hamiltonian parameters of the Frenkel pairs for which J is measured directly. For X_4 and X_8 , ^{77}Se hyperfine interactions are also resolved, see text. The principal axes are indicated in Fig. 1.

Spectrum	$ J $ (MHz)	$\mathbf{g}_h, \mathbf{g}_e$	\mathbf{D} (MHz)	Anneal T (K)	λ_{\max} (nm)
X_1	57050	$g_{h1}=1.9374$ $g_{h2}=2.2085$ $g_{h3}=2.2085$ $\tau_h=0^\circ, \mathbf{g}_l$	$D_1=\pm 900$ $D_2=\pm 1350$ $D_3=\mp 2250$ $\tau_D=35^\circ$	180	800
X_2	32048	$\mathbf{g}_V, \mathbf{g}_l$	~ 0	180	
X_3	18827	$\mathbf{g}_V, \mathbf{g}_l$	~ 0	200	~ 900
X_4	15382	$\mathbf{g}_V, \mathbf{g}_l$	~ 0	200	~ 900
X_5	14624	$\mathbf{g}_V, \mathbf{g}_l$	$D_1=\pm 180$ $D_2=\mp 90$ $D_3=\mp 90$ $\tau_D=0^\circ$	200	~ 900
X_6	13823	$\mathbf{g}_V, \mathbf{g}_l$	$D_1=\pm 300$ $D_2=\mp 150$ $D_3=\mp 150$ $\tau_D=0^\circ$	200	~ 900
X_7	11833	$\mathbf{g}_V, \mathbf{g}_l$	~ 0	200	930
X_8	4752	$\mathbf{g}_V, \mathbf{g}_l$	$D_1=0$ $D_2=\pm 300$ $D_3=\mp 300$ $\tau_D=35^\circ$	200	1000
X_9^*	1964	$\mathbf{g}_V, \mathbf{g}_l$	~ 0		
X_{10}	1820	$\mathbf{g}_V, \mathbf{g}_l$	~ 0		~ 1000
X_{11}^*	1619	$\mathbf{g}_V, \mathbf{g}_l$	~ 0		
X_{12}^*	1427	$\mathbf{g}_V, \mathbf{g}_l$	~ 0		
X_{13}	1319	$\mathbf{g}_V, \mathbf{g}_l$	~ 0	200	~ 1000
X_{14}^*	909	$\mathbf{g}_V, \mathbf{g}_l$	~ 0		
X_{15}	719	$\mathbf{g}_V, \mathbf{g}_l$	~ 0	to	~ 1000
X_{16}^*	606	$\mathbf{g}_V, \mathbf{g}_l$	~ 0		
X_{17}^*	420	$\mathbf{g}_V, \mathbf{g}_l$	~ 0		
X_{18}	252	$\mathbf{g}_V, \mathbf{g}_l$	~ 0	260	~ 1000
X_{19}^*	90	$\mathbf{g}_V, \mathbf{g}_l$	~ 0		
X_{20}^*	36	$\mathbf{g}_V, \mathbf{g}_l$	~ 0		
V_{Zn}^-	~ 0	\mathbf{g}_V	~ 0	260	1100
Zn_i^+	~ 0	\mathbf{g}_l	~ 0	260	1100

orientations of the defects can be determined, their relative intensities provide a direct measure of the defect alignment.

To identify the different orientations, we adopt the following convention, which we have used in previous studies.⁷ Referring to Fig. 1, we identify the four different $\langle 111 \rangle$ axes by the letters a , b , c , or d , as indicated. We label a C_{1h} -defect orientation by two of these letters ij , which define the C_{1h} plane, and where the first letter i denotes the $\langle 111 \rangle$ axis closest to the three axis, and the second letter j , the $\langle 111 \rangle$ axis closest to the one axis. (As noted in the figure caption, the defect orientation shown is therefore bc .) For a C_{3v} defect, we need only one letter j , to indicate the one axis of the axially symmetric defect ($\tau=0$). (The particular choice of the cubic axes in the figure is, of course, arbitrary. The axes indicated differ from those we have often used in previous papers,⁷ but have been chosen so that the four circles can be considered the four selenium atoms around the

vacancy and at the same time the $[111]$ direction properly connects the central vacancy to one of its nearest bonded selenium neighbors, c .)

The electron irradiation beam was oriented parallel to the $[111]$ or $[\bar{1}\bar{1}\bar{1}]$ crystal direction. The c - $\langle 111 \rangle$ axis is therefore a unique direction as regards the defect production, while the a -, b -, and d - $\langle 111 \rangle$ directions are different but equivalent. Therefore, for a C_{1h} center, there are three inequivalent sets of defect orientations: (1) ca , cb , cd ; (2) ac , bc , dc ; and (3) ab , ba , ad , da , bd , db . For the special case of the interstitial displaced along a $\langle 100 \rangle$ direction from the vacancy, (1) and (2) become equivalent. For a C_{3v} center, with axial symmetry along a $\langle 111 \rangle$ direction, the c orientation is unique, the a , b , and d orientations being equivalent.

Table IV presents the intensity ratios measured with \mathbf{B} in the $(1\bar{1}0)$ plane for the individual defect orientations of the

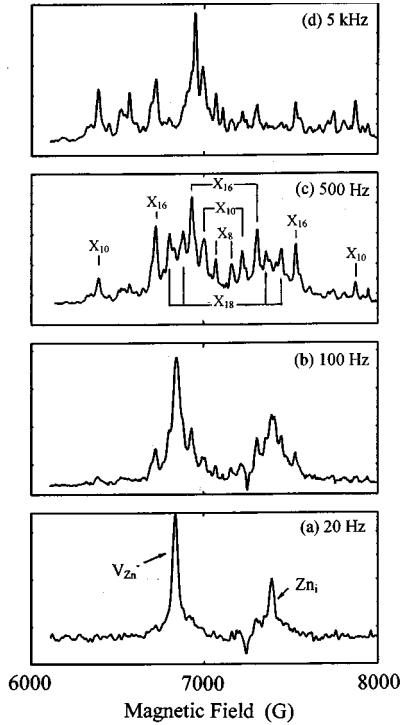


FIG. 7. ODMR spectrum in the central region, $\mathbf{B} \parallel [001]$, at four different modulation frequencies.

ODMR signals which are strong and well resolved enough for reliable measurements. All reveal preferential alignment frozen in, as expected for Frenkel pairs produced by the primary damage event. In the particular case of spectrum *B* and X_8 , the equivalence of the *ic* and *ci* orientations identifies them as pairs with the interstitial in a $\langle 100 \rangle$ direction from the vacancy.

Figure 3 includes the results of annealing for several representatives of the Frenkel pairs as does Fig. 2 for the spectral dependence of their ODMR signals. The corresponding results for all of the defects for which this information is available have been incorporated into Tables II and III.

C. Assignment of the Frenkel pairs

First, we consider correlation of the ODMR results with the previous EPR studies. The EPR signal V^I has been directly observed in shallow donor-to-Frenkel pair lumines-

TABLE IV. Alignment of the Frenkel pairs after oriented 2.5 MeV electron beam irradiation at 4.2 K.

Defect	$e^- \parallel [\bar{1} \bar{1} \bar{1}]$	$e^- \parallel [111]$
$V^I(c:b)$	(1.4 ± 0.1):1	
$A(c:b)$	(2.0 ± 0.2):1	1:(1.7 ± 0.1)
$B(ic:ci)$	(1.0 ± 0.1):1	1:(1.0 ± 0.1)
$B(dc:db)$	(1.6 ± 0.1):1	1:(1.9 ± 0.2)
$X_1(ic:ci)$		1:(1.7 ± 0.1)
$X_1(dc:db)$		1:(1.8 ± 0.1)
$X_8(ic:ci)$		1:(1.0 ± 0.1)
$X_8(dc:db)$		1:(1.8 ± 0.2)
$X_4-X_6(c:b)$		1:(no. > 1)

cence at 625 nm. Consistent with the identification, both anneal away at ~ 80 K. As described in Sec. III, it was concluded in the previous EPR study⁷ that for V^I the interstitial is 4.89 Å away from the vacancy in the easy $[\bar{1} \bar{1} \bar{1}]$ displacement direction, a site surrounded by four Se atoms.

The annealing of ODMR spectrum *A* at ~ 140 K correlates closely with that observed for V^{IV} observed in EPR,⁷ and that for spectrum *B* at ~ 180 K with that for V^{III} . In addition, the sense and magnitude of the oriented beam alignment observed for *A* and *B* in Table IV correlates closely with that observed previously by EPR (Ref. 7) for V^{IV} and V^{III} , respectively. In particular, for both *B* and V^{III} , the *ic* and *ci* intensities are identical, indicating for both an interstitial displaced in the $\langle 100 \rangle$ direction. We therefore identify *A* with V^{IV} and *B* with V^{III} , and identify *B* as being either in the nearest $\langle 100 \rangle$ position surrounded by four seleniums, at 2.83 Å, or the next such site at 8.48 Å, as proposed earlier from the EPR studies.

Beyond this it becomes difficult to assign specific zinc vacancy-zinc interstitial separations, although it is reasonable to assume a roughly monotonic decrease in exchange interaction vs separation, as we have ordered the defects in Table III. There are other indications of separation: (1) The dipole-dipole interaction should decrease with increasing separation. (2) Due to the Coulomb interaction between Zn_i^{2+} and V_{Zn}^{2-} in the ground state, annealing should result in annihilation and the annealing temperature should increase with separation. (3) The photoluminescence energy should also decrease, the maximum of each band being given by

$$E_{PL} = E_{Zn_i(+2+)} - E_{V_{Zn}(2-/-)} + \frac{3e^2}{\epsilon_0 r} - E_{relax}. \quad (14)$$

Here, the first two terms are the energy positions of the interstitial double-donor level and the vacancy double-acceptor level measured from the valence band edge, the third term approximates the Coulomb energy difference between the excited ($Zn_i^{+} + V_{Zn}^{-}$) and ground ($Zn_i^{2+} + V_{Zn}^{2-}$) states, and the last term is the energy change due to lattice relaxation differences in the ground and excited states. For pairs of different separation, the Coulomb term causes a shift to lower energies vs separation r . We note in Table III that all of these indicators are generally consistent with the indicated ordering, although there are exceptions.

One important tentative assignment has been made for spectrum X_8 ,^{3,5} which from its alignment properties indicates a $\langle 100 \rangle$ separation, like spectrum *B*. The possibility that it represents the singlet-to-triplet transitions of the same defect that gives rise to the triplet-triplet *B* transitions could be ruled out because the two have different spectral dependences, Fig. 2, and different annealing behavior, Fig. 3. There are only a limited number of interstitial sites in the $\langle 100 \rangle$ direction, all surrounded by four seleniums — one at 2.83 Å, already assigned to *B*, one at 8.48 Å, one at 14.13 Å, and continuing with 5.65 Å spacing. According to Table III, there are already more sites with larger exchange than X_8 than there are available sites closer than 8.48 Å, and we have therefore tentatively assigned X_8 to the 14.13 Å site.^{3,5} Having made this assignment, we note the reassuring fact that the

thirteen pairs of larger $|J|$, [V^I , V^{II} , $V^{III}(B)$, $V^{IV}(A)$, C , D , X_1 - X_7], account for all but three of the available closer sites (13 out of 16).

This assignment provides us with another independent estimate of the interstitial second-donor level (+/2+) position, using Eq. (14). With $E_{PL} = 1.24$ eV for X_8 , $3e^2/\epsilon_0 r = 0.35$ eV for $r = 14.1$ Å, $E_{V_{Zn}}(2-/-) = 0.66$ eV, and assuming that the major contribution to E_{relax} comes from the vacancy Jahn-Teller relaxation of 0.35 eV, we obtain

$$E_{Zn_i}(+/2+) \cong E_V + 1.90 \text{ eV} \cong E_C - 0.9 \text{ eV}. \quad (15)$$

(This is 0.1 eV deeper in the gap than our earlier estimates,^{3,5} a result of the now improved estimates for the vacancy level position and its Jahn-Teller energy.) This result is generally consistent with our approximate estimate based upon the drop off of the hyperfine interactions in Sec. IV B, of $E_C - 1.2$ eV. Being a more direct measurement, Eq. (15) represents our best estimate, assuming that the lattice position estimate is correct. From Eq. (10), this corresponds to a Bohr radius of 2.05 Å.

If **D** arose simply from distant dipole-dipole interaction between the hole on the vacancy and the electron on the interstitial, it could serve as a useful guide to separation. In the simple case of point dipoles, the interaction would be axially symmetric around the vacancy-interstitial direction in the lattice with $D_1 = -2D_2 = -2D_3 = -g_1 g_2 \mu_B^2 / r^3$. For spectra *A*, *C*, and *D* in Table IV, their D_1 values correspond to $r = 5.6$, 5.2, and 8.3 Å, respectively, which appear reasonable. However, the large departures from axial symmetry for *B*, X_1 , and X_8 , clearly point to a different mechanism, in those cases, at least. Also their large values, as well as those of X_5 and X_6 , appear somewhat out of line with the other indicators of separation. **D** can of course simply represent anisotropic exchange, and might therefore show significant oscillations and angular dependence variations depending on lattice positions due to superexchange effects, for example. Unfortunately, superexchange effects can also be expected to contribute to the isotropic exchange J , making it also a correspondingly unreliable measure of separation, by itself. In effect, we must pay attention to all separation indicators, expecting irregularities in any particular one, before detailed assignments can be made.

We will defer additional speculation as to interstitial position assignment to the following paper (II), which will probe experimentally the radiative lifetimes of the individual pairs, another indicator of separation, and will provide also a theoretical treatment of the exchange and lifetime dependences upon separation.

VI. SUMMARY

Twenty-five distinct zinc-interstitial–zinc-vacancy Frenkel pairs of different separations have been detected by ODMR in the luminescence of ZnSe after *in situ* 2.5 MeV electron irradiation at 4.2 K. For twenty of them the exchange and dipole-dipole interactions in the excited emitting state between an electron on the interstitial and a hole on the vacancy have been measured directly with high precision in the microwave transitions. Coupling this with the highly detailed information determined by EPR for some of the closer pairs,

plus ODMR studies of the isolated interstitial and EPR and ODMR studies of the isolated vacancy, makes the intrinsic defects on the zinc sublattice of ZnSe extremely well understood. We summarize briefly our present knowledge.

The isolated zinc vacancy introduces a double-acceptor level (2-/-) at $E_V + 0.66$ eV, and in its V_{Zn}^- charge state, a trigonal Jahn-Teller distortion of 0.35 eV causes the hole to localize highly in a p function on the single on-axis Se near neighbor to the vacancy. An LCAO analysis of the hyperfine interaction for this atom plus the results described in this paper for two sets of three additional Se neighbors indicates ~75% of the hole wave function on the on-axis atom with ~3% and ~5% on each of the three atoms for the other two sets. The activation energy for vacancy diffusion has been determined to be¹⁰ 1.26 ± 0.06 eV.

The isolated zinc interstitial resides on center in the T_d interstitial site surrounded by four Se atoms. Analysis of hyperfine interactions with the central Zn_i^+ atom and two shells of neighbors suggests its second-donor level (+/2+) position to be at $\sim E_C - 1.2$ eV. From a tentative identification of the separation of one of the prominent Frenkel pairs, we have obtained an independent estimate of $E_C - 0.9$ eV, generally consistent with the above value, but considered the more accurate. A luminescence band with zero phonon line at 0.907 eV has been observed which may be associated with the interstitial. It anneals in roughly the same temperature region as the interstitials seen in the ODMR, ~220–260 K, suggesting an activation energy for interstitial diffusion of ~0.6–0.8 eV. Tentative identification of interstitial zinc in the T_d site surrounded by four Zn's has also been presented, but it is unstable under optical excitation even at 4.2 K.

The twenty Frenkel pairs for which the exchange interactions have been measured have been listed in Table III and ordered by decreasing exchange, as generally expected for increasing separation. Also included are the pairs indicated as Zn_i^+ and V_{Zn}^- , for which the exchange interactions are too weak to resolve. The other indications of separation also included in the table (**D**, temperature of anneal, and wavelength of maximum emission) are also generally consistent with this ordering, although there appear to be some irregularities in **D**. All of the spectra show anisotropy, but for most of them this reflects only the anisotropy of \mathbf{g}_V and \mathbf{g}_I , the values of the isolated vacancy and interstitial, respectively, and therefore contains no information concerning specific lattice assignments. **D** potentially reflects this information, and, if it originated solely from distant dipole-dipole interaction, could be useful in this regard. However, the irregularities indicated in Tables II and III suggest other origins also present, making it less reliable. The best indicator of lattice assignment has been the alignment frozen in after irradiation along specific crystal axis directions. This has led to specific assignments for a few of the very close pairs, and also for a more distant $\langle 100 \rangle$ -oriented one that has led to the second-donor state level position estimate for the interstitial of $\sim E_C - 0.9$ eV.

In the following paper, measurements will be presented of the radiative lifetime for many of the individual Frenkel pairs. This important physical property is closely related to the overlap of the wave functions for the hole on the vacancy and the electron on the interstitial, as is the exchange, and advantage will be taken of this unique system in ZnSe to

probe what this additional information may provide. An approximate theoretical treatment of the exchange and radiative lifetime will be outlined and, with this important additional insight, tentative lattice position assignments for all of the various Frenkel pairs will be made. We will be able to argue that the assignment that has led here to the $E_C - 0.9$ eV estimate for the Zn_i^+ / Zn_i^{2+} level position is consistent with the calculations.

ACKNOWLEDGMENTS

This research has been supported jointly by the National Science Foundation under Grant Nos. DMR-80-21065, DMR-85-20269, DMR-89-02572, and DMR-92-04114, and the Office of Naval Research Electronics and Solid State Program under Grant Nos. N00014-84-K-0025, N00014-90-J-1264, and N00014-94-I-0117.

*Present address: 8 Fire Lane, Voorhees, NJ 08043.

†Present address: Department of Physics, Oregon State University, Corvallis, OR 97331.

‡Present address: Department of Physics, Trinity College, Dublin 2, Ireland.

¹F. Rong and G. D. Watkins, Phys. Rev. Lett. **58**, 1486 (1987).

²F. Rong and G. D. Watkins, Phys. Rev. Lett. **56**, 2310 (1986).

³F. Rong, W. A. Barry, J. F. Donegan, and G. D. Watkins, Phys. Rev. B **37**, 4329 (1988).

⁴F. Rong and G. D. Watkins, Mater. Sci. Forum **10-13**, 827 (1986).

⁵G. D. Watkins, F. Rong, W. A. Barry, and J. F. Donegan, in *Defects in Electronic Materials*, edited by M. Stavola, S. J. Pearton, and G. Davies, MRS Symposia Proceedings No. 104 (Materials Research Society, Pittsburgh, 1988), p. 3.

⁶W. A. Barry and G. D. Watkins, Phys. Rev. B **54**, 7789 (1996). Immediately following the present paper, this is referred to in the text as II.

⁷G. D. Watkins, in *Lattice Defects in Semiconductors 1974*, edited by F. A. Huntley, IOP Conf. Proc. No. 23 (Institute of Physics and Physical Society, London, 1975), p. 338.

⁸G. D. Watkins, Radiat. Eff. **9**, 105 (1971).

⁹G. D. Watkins, in *Defects in Semiconductors, 1972*, edited by J. E. Whitehouse, IOP Conf. Proc. No. 16 (Institute of Physics and Physical Society, London, 1972), p. 228.

¹⁰G. D. Watkins, in *Radiation Effects in Semiconductors 1976*, ed-

ited by N. B. Urli and J. W. Corbett, IOP Conf. Proc. No. 31 (Institute of Physics and Physical Society, London, 1977), p. 95.

¹¹K. M. Lee, Ph.D. dissertation, Lehigh University, 1984.

¹²K. M. Lee, LeSi Dang, and G. D. Watkins, Solid State Commun. **35**, 527 (1980).

¹³K. M. Lee, LeSi Dang, and G. D. Watkins, in *Defects and Irradiation Effects in Semiconductors 1980*, edited by R. R. Hasiguti, IOP Conf. Proc. No. 59 (Institute of Physics and Physical Society, London, 1981), p. 353.

¹⁴D. Jeon, H. P. Gislason, and G. D. Watkins, Mater. Sci. Forum. **10-12**, 851 (1986).

¹⁵D. Y. Jeon, H. P. Gislason, and G. D. Watkins, Phys. Rev. B **48**, 7872 (1993).

¹⁶A. K. Koh and D. J. Miller, At. Data Nucl. Data Tables **33**, 235 (1985).

¹⁷A. Abragam, *The Principles of Nuclear Magnetism* (Oxford University Press, London, 1961), p. 66.

¹⁸G. D. Watkins, Phys. Rev. Lett. **33**, 223 (1974).

¹⁹G. D. Watkins and J. W. Corbett, Phys. Rev. **134**, A1359 (1964).

²⁰H. Seidel and W. C. Wolf, in *Physics of Color Centers*, edited by W. B. Fowler (Academic Press, New York, 1968), p. 565.

²¹B. S. Gourary and F. J. Adrian, Phys. Rev. **105**, 1180 (1957).

²²E. Clementi and C. Roetti, At. Data Nucl. Data Tables **14**, 177 (1974).

²³*Physics of II-VI and I-VII Compounds, Semimagnetic Semiconductors*, edited by O. Madelung, Landolt-Börnstein, New Series, Group III, Vol. 17, Pt. b (Springer-Verlag, Berlin, 1982), p. 149.